

# Transverse magnetic defect-modes in two-dimensional triangular lattice photonic crystals

N. Stojić <sup>1</sup>

*Department of Physics and Astronomy  
State University of New York at Stony Brook  
Stony Brook, NY 11794-3381  
(e-mail nstojic@grad.physics.sunysb.edu)*

J. Glimm <sup>1</sup>, Y. Deng <sup>1</sup>

*Department of Applied Mathematics and Statistics  
State University of New York at Stony Brook  
Stony Brook, NY 11794-3600  
(e-mail glimm, deng, @ams.sunysb.edu)*

<sup>1</sup> *Center for Data Intensive Computing,  
Brookhaven National Laboratory*

*Building 463B*

*Upton, NY 11973-5751*

J. W. Haus

*Electro-Optics Program  
The University of Dayton  
Dayton, OH 45469-0254  
(e-mail Joseph.Haus@notes.udayton.edu)*

(December 8, 2000)

Abstract

We present a numerical study of the localized transverse magnetic defect modes in a two-dimensional, triangular-lattice photonic crystal. The sample consists of an array of circular, air-cylinders in a dielectric medium (GaAs). The defect modes were calculated by using a parallel version of the finite-difference time-domain method on the Yee mesh. To validate our computations the results for the transverse electric case were checked against experimental results and the numerical results using a different method. We study the spatial symmetry for TM modes, obtained by changing the dipole excitation frequency. Also, we vary the defect-cylinder radius to tune the resonant frequency across the band gap. The TM mode is found to be highly localized at the defect in the photonic lattice.

## I. INTRODUCTION

Photonic crystals are a novel class of optical materials fabricated with at least two different dielectric permittivities in a periodic arrangement. They have the ability to suppress, enhance, or otherwise control the emission of light in a selected frequency range by altering the density of states. A complete photonic band gap (PBG), i.e. a range of frequencies for which light cannot propagate through the crystal in any direction, is a spectral region where the density of states in an infinite crystal vanishes. Interest in photonic crystals has grown, since attention was independently directed to their unusual electromagnetic properties by Yablonovitch and John in 1987 [1], [2]. A defect in the sample can embed a local mode whose resonant frequency appears inside the band gap. The field energy is also confined to a region close to the defect. This defect mode acts like a cavity and its electromagnetic emission rate can be calculated by applying Fermi's Golden rule, which establishes a proportionality relation between the emission rate and the product of the mode density and of the matrix element for the field-atom interaction.

Subsequent developments in the field produced many potential applications based on a new basic features of photonic crystals: the symmetry of the eigen-modes, the resonance localization of light in a bulk material, and the suppression of spontaneous emission. The latter two properties are a consequence of a complete PBG. Emission rate calculations motivate further investigations of localized eigen-modes of the radiation field. Especially interesting is to achieve a high quality factor ( $Q$ ) and confine the mode to a small volume [3]. These properties can be realized by introducing a defect in a photonic microstructure [8].

In this paper we simulate numerically the electromagnetic radiation process by placing an oscillating dipole moment into the photonic crystal. Photonic crystals may also be applied to the design of low threshold lasers. The dipole placed in or near the dielectric defect radiates into the lasing mode. The results provide the eigen-mode symmetry and profile in the active region of the laser. Previous calculations on defect modes have used a number of numerical

techniques: plane-wave expansion methods [4], [15], [6], finite difference algorithms based on the scalar wave equation [7], and finite-difference time domain methods [8]. We developed a parallel version of the finite difference-time domain method, which can equally well deal with complex geometries and finite boundaries. In addition, we present a detailed study of a TM defect mode.

The underlying theory and the computational methods used in calculating the electromagnetic field are discussed in the following section. Our program is validated by a calculation of a transverse electric defect mode for a square and triangular lattice of dielectric rods. In these cases both theoretical and experimental results are available. We show agreement among our results, experiment, and previously published result. In Section 3 we examine the TM defect modes of a triangular lattice of air-rods. Two defect modes are identified corresponding to the  $E_1$  and  $B_2$  symmetry for the  $C_{6v}$  point group. We examine the dependence of the resonance frequency and energy localization in the neighborhood of the defect with defect radius. Special attention has been given to observations of defect-mode localization (measured as the field energy in a central, defect photonic lattice cell). This is the property that ultimately determines the applicability of these modes and structures to photonic devices (as it is closely related to the Q-factor in finite structures).

## II. METHODS OF CALCULATION

The theory of dipole radiation in arbitrary photonic crystals has been developed by Sakoda and Ohtaka [9], based on a Green's function formalism. Our analysis starts with Maxwell's equations:

$$\nabla \cdot \{\epsilon(\mathbf{r})\mathbf{E}(\mathbf{r}, t) + 4\pi\mathbf{P}_d(\mathbf{r}, t)\} = 0, \quad (1)$$

$$\nabla \cdot \mathbf{H}(\mathbf{r}, t) = 0, \quad (2)$$

$$\nabla \times \mathbf{E}(\mathbf{r}, t) = -\frac{1}{c} \frac{\partial}{\partial t} \mathbf{H}(\mathbf{r}, t), \quad (3)$$

$$\nabla \times \mathbf{H}(\mathbf{r}, t) = \frac{1}{c} \frac{\partial}{\partial t} \{\epsilon(\mathbf{r}) \mathbf{E}(\mathbf{r}, t) + 4\pi \mathbf{P}_d(\mathbf{r}, t)\}, \quad (4)$$

where  $\epsilon(\mathbf{r})$  denotes the position-dependent dielectric constant of the photonic lattice.  $\epsilon(\mathbf{r})$  is a periodic function except for disorder caused by dielectric defect.  $\mathbf{P}_d(\mathbf{r}, t)$  is the polarization field of the oscillating dipole, whose explicit complex form is:

$$\mathbf{P}_d(\mathbf{r}, t) = \mu \delta(\mathbf{r} - \mathbf{r}_0) \exp(-i\omega t). \quad (5)$$

Here,  $\mu$ ,  $\mathbf{r}_0$ , and  $\omega$ , are the electric dipole moment, dipole's position vector, and the angular driving frequency, respectively.  $\delta$  denotes the Dirac delta function.

The method developed for regular lattices can be applied to our problem, adding the defect mode to the extended Bloch states. Hereafter,  $\mathbf{E}_d(\mathbf{r})$  stands for the eigen-function of the defect mode and  $\omega_d$  for its eigen-angular frequency. With the assumption that  $\omega$  is close to  $\omega_d$  and neglecting the contribution from all other modes, the complex electric field in presence of the defect is:

$$\mathbf{E}(\mathbf{r}, t) \simeq -\frac{2\pi\omega_d \{\mu \cdot \mathbf{E}_d^*(\mathbf{r}_0)\} \mathbf{E}_d(\mathbf{r}) \exp(-i\omega t)}{V(\omega - \omega_d + i\Gamma)}, \quad (6)$$

where  $\mathbf{E}_d$  is the normalized electric field:

$$\int_V \epsilon(\mathbf{r}) |\mathbf{E}_d(\mathbf{r}_0)|^2 d\mathbf{r} = V. \quad (7)$$

In Eq. 6,  $\Gamma$  is the decay rate of the defect mode.  $V$  is the volume over which periodic boundary conditions are imposed. The electromagnetic energy  $U$  emitted per unit time by the oscillating dipole placed at  $\mathbf{r}_0$  is found from the expression (see [9]):

$$U \simeq -\frac{\pi\omega_d^2\Gamma|\boldsymbol{\mu}\cdot\mathbf{E}_d(\mathbf{r}_0)|^2}{V\{(\omega-\omega_d)^2+\Gamma^2\}}. \quad (8)$$

From the last equation it follows that the frequency dependence of  $U$  determines the eigen-angular frequency of the defect mode  $\omega_d$  as the resonant frequency. We developed a numerical procedure to find the frequency dependence of  $U$ .

We apply the finite-difference time-domain method to solve Maxwell equations (Eq. 1 - 4). More specifically, we applied the non-dissipative Yee's algorithm with a duality relation between the spatial representations of the electric and magnetic fields that represents both the differential and integral forms of Maxwell equations, Ref. [10] and [11]. The Yee mesh is divergence-free with respect to the electric and magnetic fields and it is suitable for specifying field boundary conditions and singularities.

To shorten the computational run time we developed a parallel code, which was run on a Pentium III linux cluster (the results described here are obtained from runs on 31 processors). The computational domain consists of 19 photonic lattice cells in the periodic structure for  $\epsilon$  in the  $x$  and  $y$  direction and 8 mesh cells in the  $z$  direction. Each photonic lattice cell has been divided into  $40 \times 40$  computational mesh cells, but due to duality of the discretization mesh (see [10]), effectively we determined each field on only  $20 \times 20$  points inside a photonic lattice cell. Periodic boundary conditions were used in all three directions. Each period of oscillation was divided into 90 time steps for the numerical integration. A typical 50-period run (about 4500 time steps) required 50 minutes of run time.

The vector electromagnetic field in the 2D photonic lattice can be decoupled into two independent modes, transverse electric (TE) where the E-field is perpendicular to the plane of periodicity. The nonzero field components are  $(\mathbf{E}_z, \mathbf{H}_x, \mathbf{H}_y)$ . The transverse magnetic (TM) case has the H-field perpendicular to the plane and the nonzero field components are:  $(\mathbf{E}_x, \mathbf{E}_y, \mathbf{H}_z)$ . In our calculations we do not prescribe the mode, but choose the mode based on the orientation of the dipole. For the TE case we introduce a line of dipoles at the center of the defect. The dipole is oriented perpendicular to the photonic crystal plane.

TE defect modes have been thoroughly investigated in two-dimensional photonic lattices (square and triangular) (e.g. Ref. [7], [12], and [13]). The calculation of the TE modes in a square lattice served as a verification of our results. We found very good agreement with numerical results obtained from a discretized scalar wave equation method. Both compared very well with experimental results of McCall *et al.* [14], who fabricated a 2D square photonic lattice. The dielectric rods were circular cylinders with the radius  $R = 0.48\text{cm}$  and dielectric constant 9.0. The lattice constant was  $a = 1.27\text{cm}$ . The rods were immersed into air ( $\epsilon = 1.0$ ) for a large dielectric contrast.

The electromagnetic energy radiated by the line of oscillating dipoles as a function of the oscillation frequency is shown in Fig. 1. The lattice defect is the removal of a dielectric rod from the center of the lattice. A resonance frequency is clearly identified after 20 periods and continues to sharpen as energy continues to build up in the defect mode. A plot of the electric field profile along the  $x$ -axis in Fig. 2 shows the field is concentrated close to the defect. The resonant frequency results agree with the aforementioned results of McCall and Sakoda. The variation between our and experimental result is less than 0.6%. The field is confined to a region around the defect extending out to about three lattice constants. Similar comparison has been made for the TE modes on a triangular lattice (dielectric rods  $\epsilon = 9.0$  immersed in air,  $R = 0.48\text{cm}$ ,  $a = 1.27\text{cm}$ ) where results were as follows: Sakoda's plane-wave method resulted in a resonance at 11.05GHz [7], experiment by Smith *et al.* yielded a resonance at 11.23GHz [15], while our calculation showed a resonance at 11.29GHz. The deviation of our result from the experiment is about 0.5%.

### III. TM MODES

Since the square lattice does not have a band gap for TM modes, we model a triangular lattice containing air-holes in a dielectric matrix. A defect in the form of an air hole with a modified radius was introduced in the center of our lattice. The lattice geometry is depicted in Fig. 3.  $\epsilon_1$  is the dielectric constant of the air-rods, whose value is 1.0.  $\epsilon_2$  is the dielectric

constant of the background matrix and its value is 13.0. The results are scalable to any lattice parameter, so we quote parameters scaled by the lattice constant. We chose to make the defect hole smaller than the holes in the rest of the lattice. The orientation of the oscillating dipole can be chosen to be in  $x$ - and/or  $y$ -direction. Depending on the dipole excitation and the size of the defect rod, different modes will appear.

The band structure of TM modes is shown in Fig. 4. The calculation is based on the plane-wave expansion method with 919 basis vectors. The relative error is determined by comparing the results for different numbers of plane waves with the asymptotic value. The error depends on the band number and increases from less than 1% for the first few bands up to 6% for the eighth band. The first gap exists between the first and second bands, i.e. between 0.375 and 0.52 in normalized frequency units. The second gap observed for this set of parameters was between the seventh and eight bands. In the next few paragraphs we will describe the modes. The horizontal dashed lines delineate the band gap edges.

To illustrate that the TM modes have well defined resonance frequencies we place a line of dipoles at the center of the defect rod. The defect radius to unit cell ratio is  $r/a = 0.35$ . The dipoles are driven at different frequencies and the radiated energy is computed. Figure 5 shows the electromagnetic energy radiated as a function of the oscillation frequency. There is a resonance peak at  $a/\lambda = 0.461$  ( $a/\lambda = \omega a/2\pi c$ ); this is the eigen-frequency of the defect mode. The peak in the radiated energy spectrum is well established after 25 oscillation periods and it continues to grow and narrow with elapsed time. After 100 oscillation periods the full width at half maximum of the resonance is about 0.005, which corresponds to a Q-factor of around 100. The resonance continues to grow and narrow and we observed no saturation of the resonance width. We can conclude that the Q-factor is larger than observed after 100 oscillation periods.

The crystal has  $C_{6v}$  symmetry and therefore six irreducible representations:  $A_1$ ,  $A_2$ ,  $B_1$ ,  $B_2$ ,  $E_1$  and  $E_2$ . By changing the radius of the defect rod and the dipole orientation different defect modes with different symmetries could appear. For the defects we considered we found that two defect modes were excited. The magnetic field is plotted in Fig. 6 for a

defect air-rod radius of  $r/a = 0.35$ . This defect mode corresponds to the  $E_1$  symmetry. The H-field is concentrated in the regions with larger dielectric constant as observed for the E-field in similar cases, eg. see [18]. The defect mode was excited by dipoles oscillating along  $y$ -direction defined by Fig. 3.  $B_2$  mode has been found for smaller defect radii, Fig. 7.

Figure 8 demonstrates the TM resonances for seven different defect-radius ratios,  $r/a$ ; values of the defect radius were between 0.26 and 0.43 for this figure; the result is the radiated energy after 100 periods of oscillation. For ratios whose eigen-frequencies approached the band gap edge, radiated energy was found to rapidly decrease. The maximum energy is radiated for the frequencies near the center of the band gap, where the mode should be highly localized [18].

The resonance frequency data for defect modes is compiled in Fig. 9. Each data point is extracted from a resonance curve for one particular defect-rod radius. The local mode is confined to the PBG frequency band. The horizontal lines in the figure represent the boundaries of the band gap. As the ratio  $r/a$  increases, the frequencies of the photonic crystal modes tend to rise monotonically and linearly due to the larger air fraction and resulting lower average index. As shown in [16] and [17], the eigen-frequency is proportional to  $1/\sqrt{\epsilon_{defect}}$ . With decreasing defect radius, the effective dielectric constant at the defect increases proportionally to  $r^2$ . Hence, in our case with constant dielectric constant and variable defect radius, the eigen-frequency versus defect radius relation becomes:  $\omega_d \sim r_{defect}$ .

By rotating the orientation of the dipole by  $90^\circ$ , the second  $E_1$  defect-mode, rotated by  $90^\circ$  is found. It is degenerate with the first mode. By combining both orientations, we obtained again the same mode rotated by  $45^\circ$ . We could not excite any totally symmetric mode most likely because of the incompatible symmetries (the dipole source produces an anti-symmetric electric field). All the fields are strongly localized around the defect. The vector electric field is plotted by arrows in Fig. 10. The length of the vector is proportional to the field strength. This corresponds to  $E_1$  mode behavior of the magnetic field in Fig. 6.

Figure 11 shows the  $E_1$  mode in a second band. This is the only mode found in the second gap region. As observed previously by Sakoda and Shiroma, [16], the spatial variation of the electric fields is faster for the modes in the second gap, than for those in the first gap.

In order to compare the localization properties of  $E_1$  mode for different frequencies (i.e. ratios  $r/a$ ) the local energy at the defect is examined. This is determined by the fraction of the radiated energy concentrated at the defect unit cell. Our results are presented in Fig. 12, where the defect cell energy is expressed as a percentage of the total radiated energy. Each frequency corresponds to a certain defect-rod radius. The precise correlation between the frequency and defect-rod radius can be extracted from Fig. 9. The general position of the points shows the increase of the energy at the defect cell with the reduction of the defect radius, which confirms, once again, that electric field tends to localize in the areas with large dielectric constant.

As found in [7], the eigen-frequencies of the defect modes depend on the number of photonic crystal layers. We also calculated the resonance frequencies for different supercells and the results are given in Fig. 13. After only a few (2 - 3) photonic crystal layers the eigen-frequency reaches its asymptotic value. The mode is localized very close to the defect.

#### IV. CONCLUSION

In this paper the results of parallel numerical simulations of dipole radiation, based on the Yee's mesh finite-difference time-domain method are presented. To overcome the large computational demands of Yee's algorithm, we developed a parallel program that improved the speed of the computations with parallel efficiency of 0.7. No symmetry was assumed for the modes to reduce the lattice size. Localized TM defect modes were examined in a two-dimensional photonic crystal triangular lattice composed of air cylinders drilled into a dielectric host. The defect was varied by changing the radius of the central cylinder. To validate our new, parallel computer code, we compared our results with previously reported results of Sakoda and experiments of McCall et al. on TE modes in a square lattice with

a missing defect cylinder. We established a very good correspondence between the results obtained by different methods.

In the TM defect-mode computations we used a triangular lattice and dielectric materials that yielded a fairly large band gap for TM modes, when the dielectric constant of the medium is 13 (GaAs). The ratio of rod radius to the lattice unit cell constant,  $R/a$  is 0.48 and we considered smaller defect-rod radii in our computations. The  $E_1$  and  $B_2$  modes were found in the first PBG. In the second PBG, we found the  $E_1$  mode only. We showed the spatial distribution of the magnetic- and electric-fields and the movement of the mode resonance through the photonic band gap as the defect radius is changed. In addition, we determined the dependence of the localization (the field energy confined at the defect cell) on frequency (defect-rod radius). We also studied the dependence of the eigen-frequencies on the number of photonic lattice cells.

TM defect-modes have not been previously reported for the pure two-dimensional lattice, due to the poor convergence of the previously used plane-wave expansion methods and numerical instability of the discretization of the scalar wave equation. Figs. 12 and 13 show a surprisingly strong localization of the  $E_1$  defect mode around the defect cylinder. From this result we infer that only a few lattice cells around a defect are required for good confinement and high Q-factors.

## FIGURES

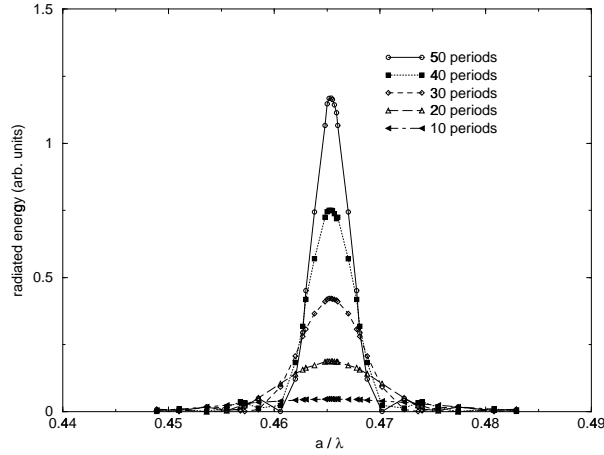


FIG. 1. The electromagnetic energy radiated versus scaled frequency for a square lattice with a defect. The radiation is emitted by a vertical, oscillating dipole moment located at the center of the grid. A rod was removed from the center of the lattice; the lattice parameters are:  $R/a = 0.378$ ,  $\epsilon_{rod} = 9$ , and  $\epsilon_{matrix} = 1$ . The labeled curves represent the energy after 10, 20, 30, 40 and 50 periods of oscillation.

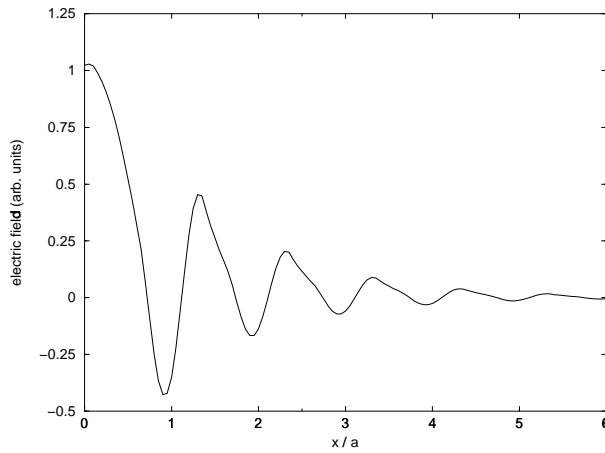


FIG. 2. The electric field as a function of the distance from the dipole after 100 periods of oscillations for  $\omega a/2\pi c = 0.467$  for the square photonic lattice with a defect. See the caption in figure 1 for details.

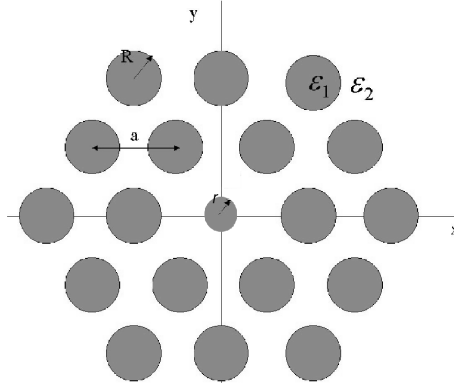


FIG. 3. The top view of the two-dimensional array of circular rods used for the calculation.  $\epsilon_1$  and  $\epsilon_2$  denote the dielectric constants of the rods or of the embedding matrix material;  $R$  and  $r$  are the radii of the lattice rods and the defect rod, respectively.  $a$  denotes the lattice constant.

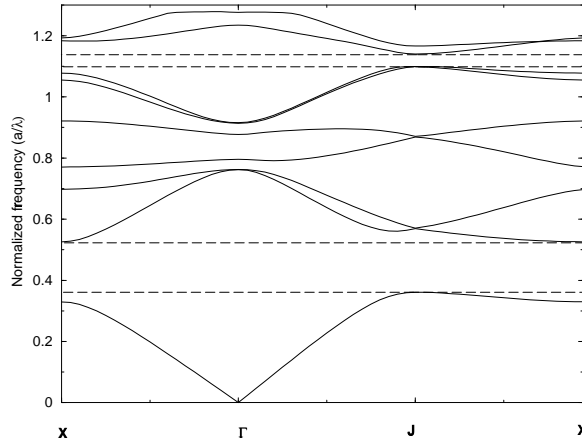


FIG. 4. The photonic band structure of the regular triangular lattice for TM polarization, where the ordinate represents the normalized frequency. This is calculated by a plane-wave expansion method using 919 basis functions. The following parameters were assumed:  $R/a = 0.48$ ,  $\epsilon_1 = 1$ ,  $\epsilon_2 = 13$ . A large band gap exists between 0.375 and 0.52 in the normalized units. The  $\Gamma - X$  direction is along the second-nearest neighbor lines through the crystal, eg. the  $y$ -direction in Fig. 3, and the  $\Gamma - X$  direction is along the nearest neighbor lines through the crystal, eg. the  $x$ -direction.

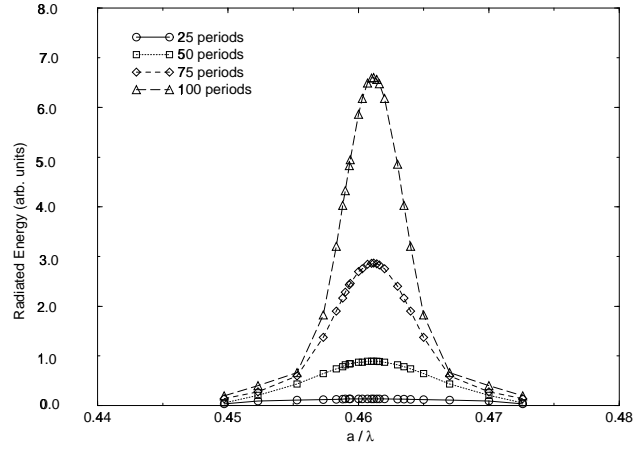


FIG. 5. The frequency dependence of the accumulated electromagnetic energy for an  $E_1$  mode radiated by an oscillating dipole at the center of the defect after 25, 50, 75 and 100 periods of oscillation. The defect rod-radius is  $r/a = 0.35$ .

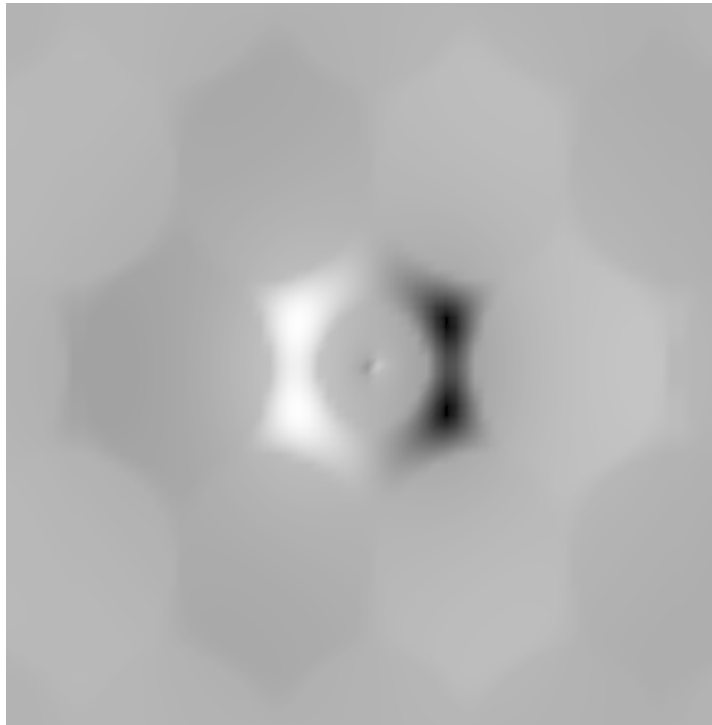


FIG. 6. The spatial distribution of the magnetic field after 100 oscillation periods at the scaled angular frequency  $\omega a/2\pi c = 0.411$ . The mode's symmetry corresponds to the  $E_1$  mode. The ratio of the defect radius to the lattice unit cell is  $r/a = 0.28$ . Dark shades correspond to negative amplitude values and light shades correspond to positive amplitude values.

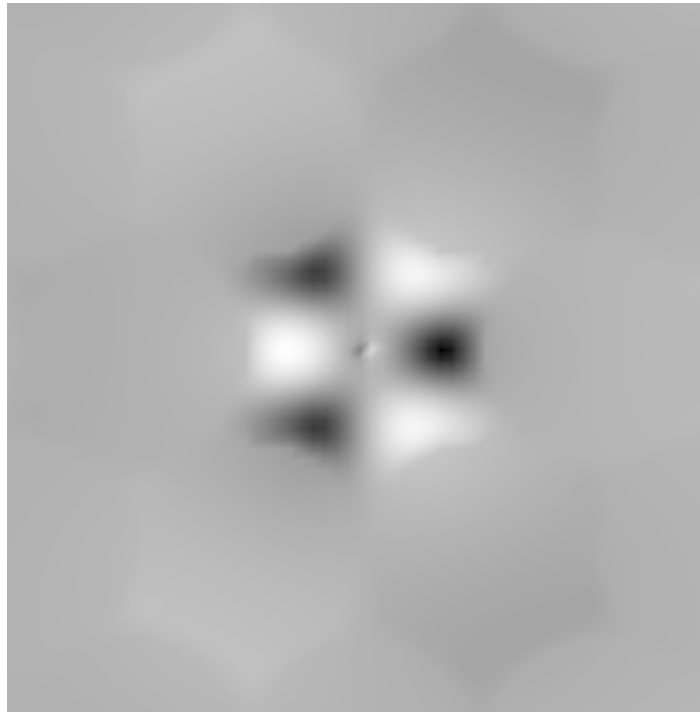


FIG. 7. The spatial distribution of the magnetic field after 100 oscillation periods at the scaled angular frequency  $\omega a/2\pi c = 0.48$ . The mode's symmetry corresponds to the  $B_2$  mode. The ratio of the defect radius to the lattice unit cell is  $r/a = 0.00$ . Dark shades correspond to negative amplitude values and light shades correspond to positive amplitude values.

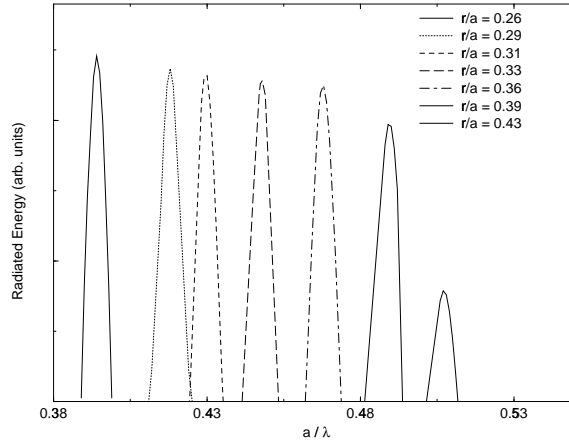


FIG. 8. The radiated electromagnetic energy for different defect-radius ratios  $r/a$  as a function of the scaled frequency.

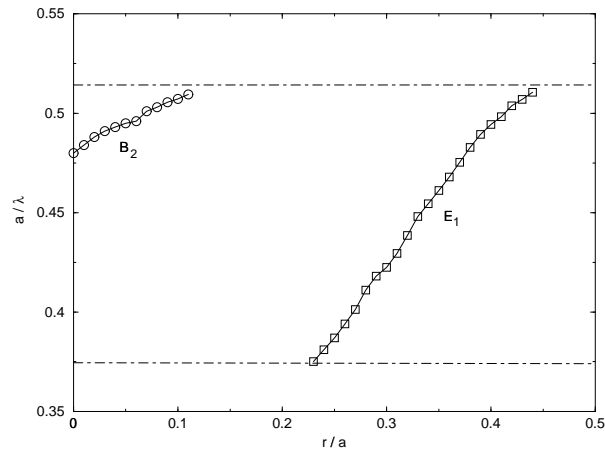


FIG. 9. The eigen-frequency of the localized defect modes as a function of the radius of the defect rod. The ordinate is the normalized frequency and horizontal lines represent the boundaries of the photonic band gap calculated from Fig. 4.

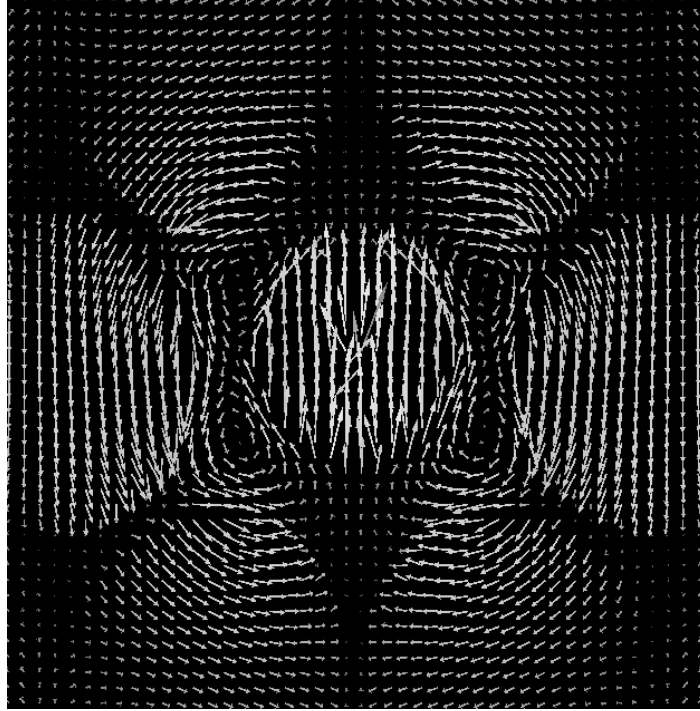


FIG. 10. The vector representation of the electric field for the  $E_1$  mode after 100 periods of oscillation at  $\omega a/2 \pi c = 0.461$ . The ratio of the defect radius to the lattice unit cell is 0.35.

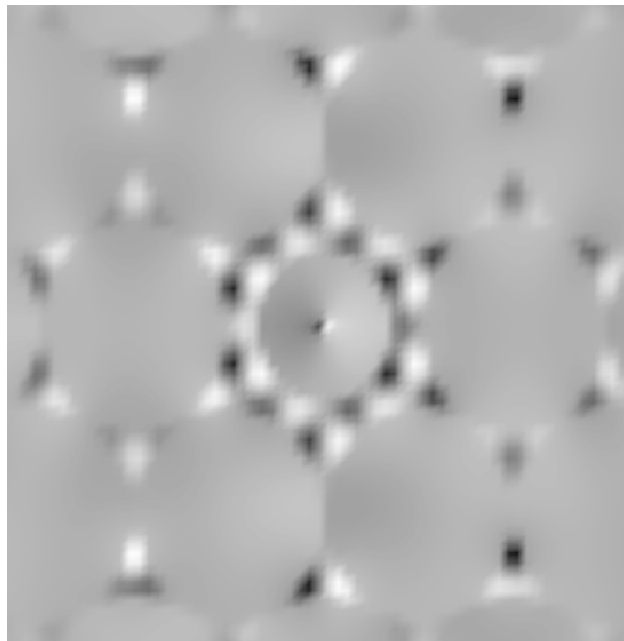


FIG. 11. The spatial distribution of the magnetic field after 100 oscillation periods at the scaled angular frequency  $\omega a/2\pi c = 1.11$  in the second band gap. The mode's symmetry corresponds to the  $E_1$  mode. The ratio of the defect radius to the lattice unit cell is  $r/a = 0.34$ . We observe higher spatial frequency variations than for the mode in the first gap. Dark shades correspond to negative amplitude values and light shades correspond to positive amplitude values.

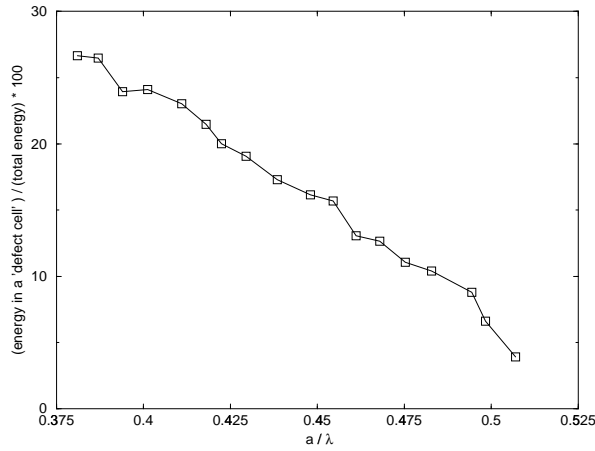


FIG. 12. The ratio of the field energy at a defect cell to the total energy as a function of resonant frequency, which is related to the defect radius.

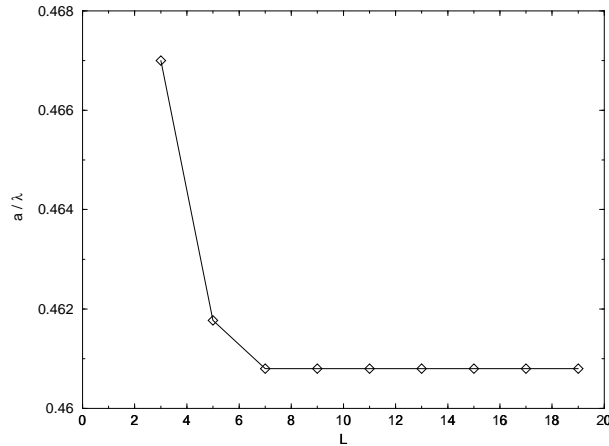


FIG. 13. The dependence of eigen-frequencies on the number of photonic lattice unit cells in  $x$  ( $y$ ) direction,  $L$ .

## ACKNOWLEDGMENTS

N. Stojić would like to thank James Davenport for helpful discussions. This work was financially supported by the United States Department of Energy department under Grant No. DE-AC02-98CH10886. J. Glimm was supported by DOE Grants DE-FG02-90ER25084, DE-FG02-989ER2536, and DE-FG03-98DP00206. JWH was supported by NSF Grant ECS-9630068.

## REFERENCES

- [1] E. Yablonovitch, *Phys. Rev. Lett.* **58**, 2486 (1987).
- [2] S. John, *Phys. Rev. Lett.* **58**, 2059 (1987).
- [3] T. F. Krauss *Prog. Quant. El.* **23**, 51 (1999).
- [4] R. D. Meade, K. D. Brommer, A. M. Rappe, and J. D. Joannopoulos *Appl. Phys. Lett.* **61**, 495 (1992).
- [5] D. R. Smith, R. Dalichaouch, N. Kroll, S. Schultz, S. L. McCall, and P. M. Platzmann *J. Opt. Soc. Am. B* **10**, 314 (1993).
- [6] X. P. Feng and Y. Arakawa *Jpn. J. Appl. Phys, Part 2* **36**, L122 (1997).
- [7] K. Sakoda, *J. Appl. Phys.* **84**, 1210 (1998).
- [8] O. Painter, J. Vuckovic, and A. Scherer, *J. Opt. Soc. Am. B* **16**, 275 (1999).
- [9] K. Sakoda and K. Ohtaka *Phys. Rev. B* **54**, 5732 (1996).
- [10] K. Yee, *IEEE Trans. Ant. Prop.* **AP-14**, 302, (1966).
- [11] A. Taflove, *Computational Electrodynamics: the finite-difference time-domain method* (Artech House, Boston, 1995).
- [12] N. Kawai, M. Wada and K. Sakoda, *Jpn. J. Appl. Phys.* **37**, 4644 (1998).
- [13] V. Kuzmiak and A. A. Maradudin, *Phys. Rev. B* **57**, 15242 (1998).
- [14] S. L. McCall, P. M. Platzman, R. Dalichaouch, D. Smith, and S. Schultz, *Phys. Rev. Lett* **67**, 3380, (1991).
- [15] D. R. Smith, R. Dalichaouch, N. Kroll, S. Schultz, S. L. McCall, and P. M. Platzman, *J. Opt. Soc. Am. B* **10**, 314 (1993).
- [16] K. Sakoda and H. Shiroma *Phys. Rev. B* **56**, 4830 (1997).

- [17] E. Yablonovitch, T. J. Gmitter, R. D. Meade, A. M. Rappe, K. D. Brommer, and J. D. Joannopoulos, *Phys. Rev. Lett.* **67**, 3380 (1991).
- [18] J. D. Joannopoulos, R. D. Meade, and J. N. Winn *Photonic Crystals* (Princeton University Press, Princeton, 1995).